



## OPEN ACCESS

## EDITED BY

Veerappan Mani,  
King Abdullah University of Science and  
Technology, Saudi Arabia

## REVIEWED BY

Mani Govindasamy,  
Ming Chi University of Technology,  
Taiwan  
Gururaj Kudur Jayaprakash,  
Nitte Meenakshi Institute of Technology,  
India

## \*CORRESPONDENCE

A. Ratnamala,  
✉ rannapra@gitam.edu,  
✉ ratnamala78@gmail.com

RECEIVED 18 April 2023

ACCEPTED 18 July 2023

PUBLISHED 01 August 2023

## CITATION

Hasheena M, Ratnamala A, Noorjahan M,  
Reddy GD and Begum G (2023),  
Hierarchical graphene oxide-Ni<sub>3</sub>S<sub>2</sub>  
quantum dots nanocomposites modified  
glassy carbon electrode for  
electrochemical detection of dopamine  
and tyrosine.  
*Front. Mater.* 10:1207875.  
doi: 10.3389/fmats.2023.1207875

## COPYRIGHT

© 2023 Hasheena, Ratnamala,  
Noorjahan, Reddy and Begum. This is an  
open-access article distributed under the  
terms of the [Creative Commons  
Attribution License \(CC BY\)](https://creativecommons.org/licenses/by/4.0/). The use,  
distribution or reproduction in other  
forums is permitted, provided the original  
author(s) and the copyright owner(s) are  
credited and that the original publication  
in this journal is cited, in accordance with  
accepted academic practice. No use,  
distribution or reproduction is permitted  
which does not comply with these terms.

# Hierarchical graphene oxide-Ni<sub>3</sub>S<sub>2</sub> quantum dots nanocomposites modified glassy carbon electrode for electrochemical detection of dopamine and tyrosine

M. Hasheena<sup>1</sup>, A. Ratnamala<sup>1\*</sup>, M. Noorjahan<sup>2</sup>, G. Deepthi Reddy<sup>2</sup> and Gousia Begum<sup>1</sup>

<sup>1</sup>Department of Chemistry, GITAM University, Hyderabad, India, <sup>2</sup>Department of Chemistry, Palamuru University, Mahbubnagar, Telangana, India

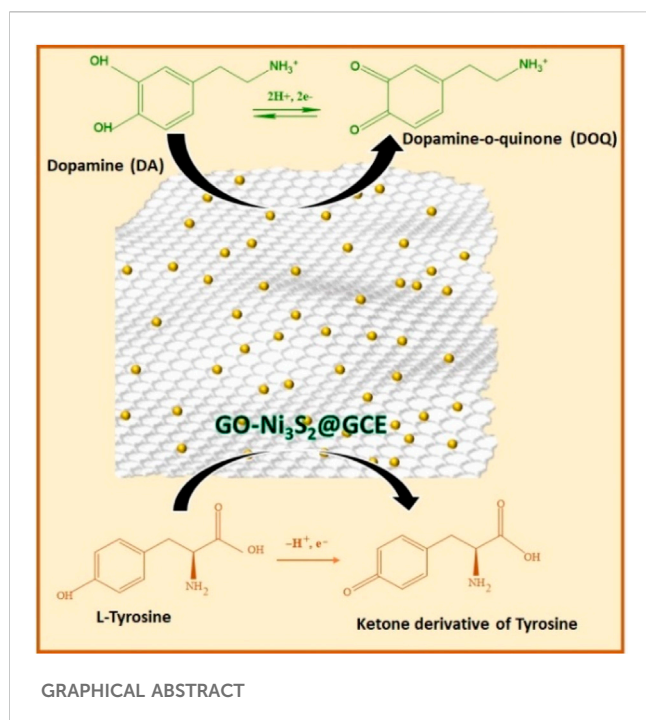
A facile synthetic strategy is demonstrated to generate nickel sulfide quantum dots (Ni<sub>3</sub>S<sub>2</sub>). The thus formed Ni<sub>3</sub>S<sub>2</sub> quantum dots are assembled onto exfoliated graphene oxide sheets hydrothermally to form nickel sulfide-graphene oxide nanocomposite material (GO-Ni<sub>3</sub>S<sub>2</sub>). The microscopic and spectroscopic characterization of the GO-Ni<sub>3</sub>S<sub>2</sub> nanocomposites revealed the shape, size, crystalline phases, and oxidation states (of elements) of the hybrid material. The GO-Ni<sub>3</sub>S<sub>2</sub> nanocomposites are then coated onto the glassy carbon electrode by drop casting to form GO-Ni<sub>3</sub>S<sub>2</sub>@GCE. The modified electrode is then used to detect dopamine and tyrosine simultaneously. The effect of scan rate, analyte concentrations, pH, and interfering agents on the peak current are studied to establish a plausible mechanism for oxidizing dopamine and tyrosine at GO-Ni<sub>3</sub>S<sub>2</sub>@GCE. The GO-Ni<sub>3</sub>S<sub>2</sub>@GCE is stable for 3 weeks and ten cycles of washing with minimal loss in the peak current in each cycle. Dopamine with a concentration as low as 12 nM can be detected using the GO-Ni<sub>3</sub>S<sub>2</sub>@GCE system.

## KEYWORDS

quantum dots, dopamine, tyrosine, electrochemical detection, cyclic voltammetry

## Highlights

- A green method for the synthesis of nickel sulphide quantum dots and their assembly onto graphene oxide sheets is demonstrated.
- The nickel sulphide-graphene oxide nanocomposite material is coated on a glassy carbon electrode and used for the simultaneous detection of dopamine and tyrosine.
- There was a 50% increase in the electroactive surface area of the modified glassy carbon electrode compared to that of the bare glassy carbon electrode.
- The electrochemical studies indicate that the lowest detection limit of dopamine is 12 nM.
- The mechanism for electron transfer in the analyte at the modified electrode is established by varying the reaction parameters.
- The stability and repeatability test indicated that the nickel sulphide-graphene oxide nanocomposite coated on a glassy carbon electrode is stable for 3 weeks and 10 washing cycles with a minimal current drop in each cycle.



## 1 Introduction

The technical advancement of medical diagnostic tools has made significant strides throughout the years. In terms of early identification of ailments like diabetes, cancer, and neurological disorders commonly linked to metabolic issues, the existing diagnostic procedures have several limitations (Kapalka, 2010). The concentrations of specific biomarkers like dopamine, ascorbic acid, and tyrosine in the blood are connected to metabolic problems; accurately determining their concentrations is critical to identifying such disorders. Tyrosine (Tyr) is a biological precursor of dopamine and norepinephrine and is a non-essential aromatic amino acid created when phenylalanine is hydroxylated. It is involved in the production of melanin, thyroxine, and adrenaline and is a cause of genetic, hormonal, and neurological diseases. Tyrosine metabolism anomalies generate several inborn diseases, including Tyrosinemia I, II, and III, Hawkinsinuria, and Alkaptonuria (AKU) (Furukawa et al., 2008; Kapalka, 2010; Khadjavi et al., 2015; Mohorko et al., 2015; Turyan et al., 2018). As tyrosine is a neurotransmitter and a member of the catecholamine family, its levels in the body are one of the determining variables in mental illnesses such as anxiety and mood swings. The level of tyrosine in blood tissue may be used as a litmus test to anticipate and gauge the severity of metabolic diseases such as type II diabetes, insulin resistance, obesity, and liver cancer (Ferguson et al., 2013). Dopamine (DA), a neurotransmitter from the catecholamine family, is crucial for transmitting signals between neurons. Excess dopamine can lead to illnesses including Huntington's, schizophrenia, and Parkinson's disease, among others (Dalley and Roiser, 2012; Owesson-White et al., 2012; How et al., 2014; Xia et al., 2016; Cheng et al., 2017; Devi et al., 2018; Fazio et al., 2018; Kim et al., 2018; Üge et al., 2018).

The analytical methods for identifying tyrosine (Alonso et al., 2003; Huang et al., 2006; Ishii et al., 2006; Lee and Yang, 2006) and dopamine (Carrera et al., 2007; Chen et al., 2011; Khattar and Mathur, 2013; Ghodsi et al., 2015; Leng et al., 2015; Nurzulaikha et al., 2015; Schumacher et al., 2015; Gao et al., 2017; Shen et al., 2017) in biological fluids, including chromatography, fluorescence, mass spectrometry, and other approaches, are only partially efficient because of their intrinsic limitations. Due to rapid response, accuracy, and mobility, electrochemical techniques using electrochemical sensors (Danielle et al., 2012) are very promising in accurately detecting these biomolecules that coexist in biological fluids (Manjunatha et al., 2009; Jackowska and Kryszinski, 2013; Bhakta et al., 2015; Zahra et al., 2019). One of the challenges is usually interference brought on by a high concentration of uric acid and ascorbic acid (AA, 100–1,000 times more abundant than DA), which is mostly found in the central nervous system and has an oxidation potential that is near to that of DA. In sensing biomolecules, the bare electrodes cannot distinguish or differentiate the potentials, but the electroactive species undergo oxidation and give out an oxidation current as an analyte signal. Chemically modifying the bare electrode surfaces is one approach to solving this issue. It is well-known that materials like carbon, conducting polymers, and metal oxide nanoparticles are desirable for modifying bare electrode surfaces because they can separate the oxidation potentials of electroactive molecules and measure their concentration as a function of oxidation current. The materials employed for modification should also strengthen or magnify the current produced by the oxidation of the electroactive molecules. Utilizing various materials, including metal nanoparticles, conducting polymers, and carbon, customized electrodes have been used to measure dopamine, tyrosine, and ascorbic acid (Wan and Zhiqiang, 2015; Tooley et al., 2018). One such material is graphene oxide which contains a variety of defect shapes, also there are oxygen-containing groups like epoxides and hydroxyls are present. These oxygen and defects assist in lowering the overpotential connected with biosensing by increasing the density of electronic states at the Fermi level. The enormous surface area of 2D graphene sheets, which enables the loading of additional biomolecules onto the surface, is another important characteristic. They can also function as effective electron mediators, promoting electron transport between the electrode surface and the metal active sites of the biomolecules. Hence in the present study graphene oxide is chosen to enhance sensing capability along with metal sulphide. Numerous electrochemical sensors that measure amino acids, neurotransmitters, carbohydrates, and other biomolecules have also been developed using NiO nanoparticles (Dong et al., 2011; Yang J. et al., 2013; Yang L. et al., 2013; Liu et al., 2014; Zhao et al., 2018; Khan et al., 2022). Metal sulphides and more precisely various phases of nickel sulphides are mainly used in battery and supercapacitor applications and reports on sensors is very rare (Zhao et al., 2018; Khan et al., 2022).

The development of electrochemical sensors using graphene, MWCNT, reduced graphene, *etc.* (Cheng et al., 2020) is still piquing researcher's interest even though much research is being done on carbon-based materials. Lee et al. has reported cetyl pyridinium bromide (CPB) modified carbon paste electrode (CPBMCPE) employed for detection of dopamine (DA) and

uric acid (UA) with good selectivity and sensitivity. Their theoretical studies reveal that the charged cationic head of CPBs can offer an additional electron transfer site at the CPBMCPPE interface might enhanced the sensing ability. (Jayaprakash et al., 2020).

These graphene oxide materials have unique properties like high surface area, excellent electrical conductivity, high charge carrier mobility, and quantum hall effect. It is reported in literature that GO is used as support for detecting chemotherapeutic drugs (Tseng et al., 2020), determination of DNA detecting biomarkers (Govindasamy et al., 2019), detecting sulphasalazine (Rajaji et al., 2022) detection of hexestrol (Govindasamy et al., 2023) detection of anti-rheumatic drugs (Rajaji et al., 2021) also used for detection of organoarsenic roxarsone (Tamilalagan et al., 2023) In the current study, graphene oxide-nickel sulphide (GO-Ni<sub>3</sub>S<sub>2</sub>) nanocomposites are generated using ultrasonication and hydrothermal processes. The simultaneous detection of DA and Tyr is then performed using the graphene oxide-nickel sulfide-modified glassy carbon electrode (GO-Ni<sub>3</sub>S<sub>2</sub>@GCE). We anticipate that the facile synthetic strategy can be explored for the design of hybrid materials for applications in energy to biomedicine.

## 2 Experimental

### 2.1 Materials

Nickle chloride (NiCl<sub>2</sub>·6H<sub>2</sub>O), sodium sulfide flakes, potassium chloride, ascorbic acid, uric acid, and sodium phosphate (mono and di sodium) were procured from SD Fine Chemicals, INDIA. Dopamine and graphene oxide were purchased from Sigma-Aldrich. Tyrosine was bought from Fischer Scientific Ltd., and all the chemicals used in this work were used as received.

### 2.2 Instruments

The produced GO-Ni<sub>3</sub>S<sub>2</sub> quantum dots were examined using a variety of characterization techniques. The X'pert Pro X-ray diffractometer was used to investigate the size of GO-Ni<sub>3</sub>S<sub>2</sub> quantum dot phases and crystallinity using Ni-filtered Cu K $\alpha$  radiation ( $\lambda = 1.5406$ ,  $2\theta = 0-60^\circ$  analytical B.V., Netherlands). The surface morphology of the GO-Ni<sub>3</sub>S<sub>2</sub> quantum dots was captured using scanning electron microscopy (ZEISS EVO 18 model) at a voltage of 40 kV and a current of 30 mA @ 0.388 scans per minute. Using a Quanta Chrome NOVA 1000 surface analyzer at 196 °C, the textural characteristics of GO-Ni<sub>3</sub>S<sub>2</sub> quantum dots were examined for nitrogen adsorption testing. To remove pre-absorbed gas and moisture, samples were degassed at 300 °C for 4 h before testing. The BET method was used to compute the cumulative diameter and volume of pores, and the BJH method was used to quantify the amount of nitrogen absorbed from the desorption isotherms.

GO-Ni<sub>3</sub>S<sub>2</sub> quantum dots were seen using an FEI TECHNAI G2 transmission electron microscope, and their selected area electron diffraction (SAED) patterns were obtained (TEM). Before TEM imaging, a tiny drop of the sample solution was applied to a particular 3-mm carbon-coated copper grid and allowed to dry at ambient temperature. Colloidal dispersions of GO-Ni<sub>3</sub>S<sub>2</sub> quantum dots at a lower concentration (0.001M) were measured in the 200–1,100 nm

wavelength range using a UV-1800 PC Shimadzu spectrophotometer. X-ray photoemission spectra were captured on a KRATOS AXIS 165 using Mg K $\alpha$  radiation (1,253.6 eV) at 75 W and a hemispherical analyzer coupled to a five-channel detector. The background pressure was kept at or below 10–10 bar while data was being collected. The C 1s line at 284.6 eV was used as an internal standard to correct binding energies. In each case, symmetric gaussian shapes were used. Binding energies were generally consistent within  $\pm 0.1$  eV for identical samples.

### 2.3 Synthesis of mixture of nickel sulfide (NiS/Ni<sub>3</sub>S<sub>2</sub>) quantum dots

Nickel Sulfide quantum dots were synthesized using a modified two-step method, as described in our reported work (Qi et al., 2016). The fresh *Syzygium cumini* (*S. cumini*) leaves (100g) were cleaned using distilled water multiple times to eliminate foreign particles and was then pulverized using a mortar and pestle. The *S. cumini* extract was diluted with distilled water and agitated for 30 min, followed by filtration using Whatman filter paper. The filtrate was stored in sealed bottles in the refrigerator and diluted with distilled water before use.

A 0.1 M Nickel Chloride solution (final concentration) was added to 250 mL of hot *S. cumini* leaf extract and stirred. After 5 min, Na<sub>2</sub>S (0.1M) was added portion wise with continuous stirring for 30 min. The solid formed was centrifuged and rinsed with water and ethanol before being dried in an oven at 65 °C for 8 h.

### 2.4 Synthesis of graphene oxide-nickel sulphide (GO-Ni<sub>3</sub>S<sub>2</sub>) nanocomposites

The synthesis of graphene oxide-nickel sulphide nanocomposite materials was performed by ultrasonication followed by the hydrothermal technique. An ultrasonic bath was used to homogenize 500 mg of graphene oxide (GO) in 100 mL of distilled water in a beaker. The homogeneous GO solution was added to preformed nickel sulfide, followed by hydrothermal treatment for 24 h at 100 °C. The resulting colloidal solution was washed with water and ethanol before being aged in a beaker for around 12 h. The solid thus obtained was dried in an oven at 65 °C for 24 h.

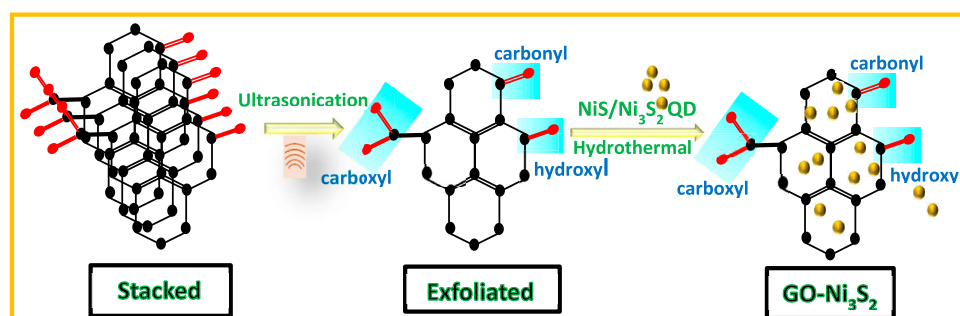
### 2.5 Electrode preparation

The glassy carbon electrode (GCE) was washed with distilled water and polished using an alumina polishing pad. The 5 mg of GO-Ni<sub>3</sub>S<sub>2</sub> was dispersed in 1 mL DML by sonication for 15 min. A thin layer of GO-Ni<sub>3</sub>S<sub>2</sub> was formed onto the electrode by drop casting, followed by drying at room temperature for 24 h.

## 3 Results and discussion

### 3.1 Synthesis

A green synthesis method was utilized for the synthesis of Nickel sulphide quantum dots containing mixture of NiS/Ni<sub>3</sub>S<sub>2</sub> phases,



SCHEME 1

Illustration of synthetic strategy to prepare GO-Ni<sub>3</sub>S<sub>2</sub> nanocomposites.

which were then assembled onto the GO sheets. The stacked GO sheets were exfoliated by ultrasonication, and the mixture of NiS/Ni<sub>3</sub>S<sub>2</sub> quantum dots were then built on it hydrothermally to generate GO-Ni<sub>3</sub>S<sub>2</sub> nanocomposite predominately (Scheme 1).

## 3.2 Characterization

The scanning electron microscopic (SEM) image revealed the sheet-like structure of GO (Figure 1A). The transmission electron microscopic (TEM) image showed the highly dispersed Ni<sub>3</sub>S<sub>2</sub> quantum dots of 2–3 nm size (as indicated by red arrows) decorated on sheet-like GO (Figure 1B). The selected area electron diffraction (SAED) pattern reflected the crystalline nature of Ni<sub>3</sub>S<sub>2</sub> quantum dots with a hexagonal phase (Figure 1C).

The X-ray diffraction pattern of the GO-Ni<sub>3</sub>S<sub>2</sub> quantum dots exhibited diffraction patterns corresponding to the hexagonal phase of Ni<sub>3</sub>S<sub>2</sub> (JCPDS card No. 44–1,418) at  $2\theta = 26.08$  (101), 34.09 (110), 43.40 (202), 51.72 (211), and 77.7 (131) (Figure 1D) (Zhou et al., 2018; Zou et al., 2018). The  $sp^2$  graphene oxide carbon at  $2\theta = 26.0$  and 45 coexisted with reflections from Ni<sub>3</sub>S<sub>2</sub>. Raman spectroscopy was used to analyze the interaction between GO and Ni<sub>3</sub>S<sub>2</sub>. The Raman spectra of GO-Ni<sub>3</sub>S<sub>2</sub> quantum dots exhibit two prominent peaks, corresponding to the G band (at 1,573  $cm^{-1}$ ) and the D band (at 1,347  $cm^{-1}$ ) (Figure 1E). The G-band represents the stretching vibration mode in the  $sp^2$ -hybridized C–C bonds, while the D band corresponds to the disorder of the  $sp^2$  carbonyl domain (Wu et al., 2018; Tian et al., 2019). Generally, the ratios of intensity between the D and G bands indicate the disorder degree of the graphitic layers. Here, the ID/IG ratio is higher than that of GO (1.04), suggesting a higher degree of defects in GO-Ni<sub>3</sub>S<sub>2</sub> quantum dots due to the reduction process and incorporation of the Ni<sub>3</sub>S<sub>2</sub> onto GO layers (Huang et al., 2008). The elemental analysis by energy-dispersive X-ray spectroscopy (EDS) indicated the presence of nickel, carbon, oxygen, and sulfur (Figures 1F,G). Additionally, the Ni:S atomic ratio is 8:5, which is about 3:2 and, in turn, validates the formation of Ni<sub>3</sub>S<sub>2</sub>.

The oxidation states and surface chemical functionalities, and valence states of GO-Ni<sub>3</sub>S<sub>2</sub> were examined by X-ray photoelectron spectroscopy (XPS). The wide survey spectrum revealed four elements C, O, S, and Ni (Figure 2A). The XPS patterns of C1s showed a prominent peak at a binding energy of 284.78 eV which

refers to C–C/C–O, a peak at a binding energy of 285.4 eV is attributed to C–O and 287.4 eV peak is assigned to C=O bonds (Figure 2B). The cliffs at 163.7 eV and 165.14 eV correspond to S<sup>2-</sup> and S<sub>2</sub><sup>2-</sup> states of S 2p, respectively. As acknowledged in the literature peak at 168.8 corresponds to partially oxidized sulfur species (Figure 2C) (Yang et al., 2017). The Ni 2p spectrum can be divided into two spin-orbit doublets and two shake-up satellites.

The high-resolution Ni 2p spectra indicated two peaks at Ni 2p<sub>3/2</sub> (855.6 eV) and Ni 2p<sub>1/2</sub> (873.7 eV) (Figure 2D). Furthermore, the two main peaks are deconvoluted into two spin orbit doublets and satellite peaks in which the Ni 2p<sub>1/2</sub> orbit is composed of two peaks with 873.3 eV and 875.9 eV assignable to the Ni(II) and Ni(III) oxidation states. Additionally, the Ni 2p<sub>3/2</sub> orbit is comprised of two peaks belonging to Ni(II) (855.3 eV) and Ni(III) (856.5 eV). These results indicate the existence of Nickel (II) and (III) in GO-Ni<sub>3</sub>S<sub>2</sub> quantum dots (Hou et al., 2017; Gao et al., 2018).

The N<sub>2</sub> adsorption and desorption isotherms of GO-Ni<sub>3</sub>S<sub>2</sub> quantum dots are shown in Figure 3. The adsorption isotherms are comparable to type (IV) isotherms, with a hysteresis loop in the P/P<sub>0</sub> range of 0.5–1, indicating the existence of mesopores (Zhao et al., 2017). The surface area of the Ni<sub>3</sub>S<sub>2</sub>-GO quantum dots is 1.586 m<sup>2</sup> g<sup>-1</sup>, with a pore diameter of 3.742 nm and a measured pore volume of 0.00989 cc g<sup>-1</sup>. The findings are in line with those previously published (Cheng et al., 2015).

## 3.3 Electrochemical performance of dopamine and tyrosine on the GO-Ni<sub>3</sub>S<sub>2</sub> nanocomposite modified electrode (GO-Ni<sub>3</sub>S<sub>2</sub>@GCE)

All the electrochemical experiments were performed in a three-electrode cell assembly comprising a GCE with a 3 mm diameter as the working electrode, platinum wire as the counter electrode, and an Ag/AgCl in 3 M KCl as the reference electrode. It has been a great challenge in electrochemical analytical research to simultaneously detect dopamine and tyrosine as they coexist in the blood and the interference among them and with the other biological fluids hampers the efficacy of the detection system. Moreover, the high concentration of dopamine and low concentration of tyrosine is another major limitation in the simultaneous detection of dopamine and tyrosine.

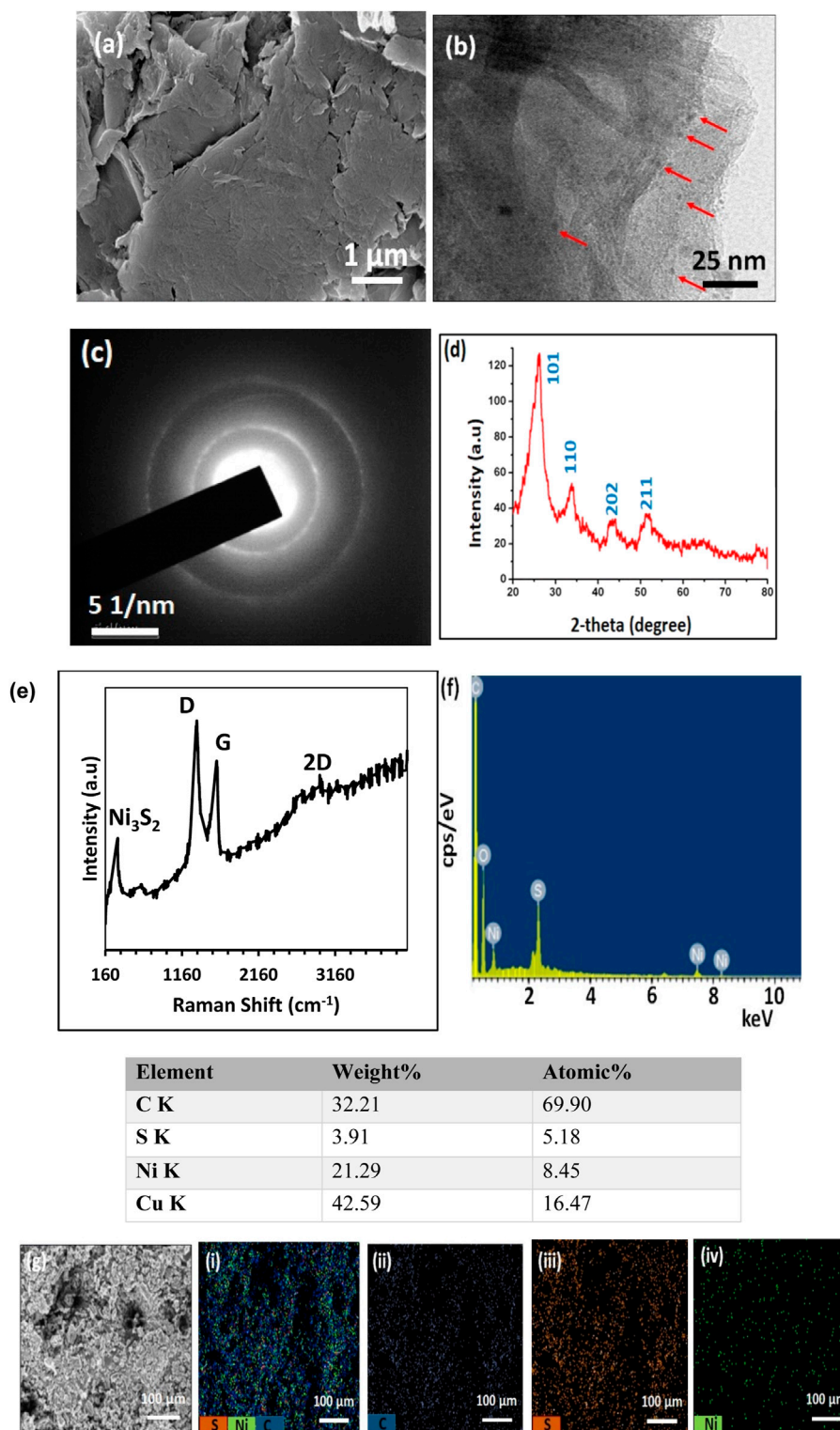


**FIGURE 1** Characterization of GO-Ni<sub>3</sub>S<sub>2</sub> nanocomposites. (A) SEM and (B) TEM images (red arrows indicate the Ni<sub>3</sub>S<sub>2</sub> quantum dots) (C) SAED pattern (D) XRD pattern (E) Raman spectrum (F) EDS spectrum with Atomic% and (G) (i-iv) Elemental mapping.

### 3.4 Electrochemical impedance studies (EIS)

The electrical properties of the produced electrodes were investigated using electrochemical impedance tests in 0.1 M KCl

at its formal potential in the frequency range 100 kHz to 100 mHz with a 10 mV amplitude. Figure 4 shows a typical EIS response of bare GCE and GO-Ni<sub>3</sub>S<sub>2</sub> coated on GCE (GO-Ni<sub>3</sub>S<sub>2</sub>@GCE). A partial semicircle with a nearly straight tail at the bare GCE

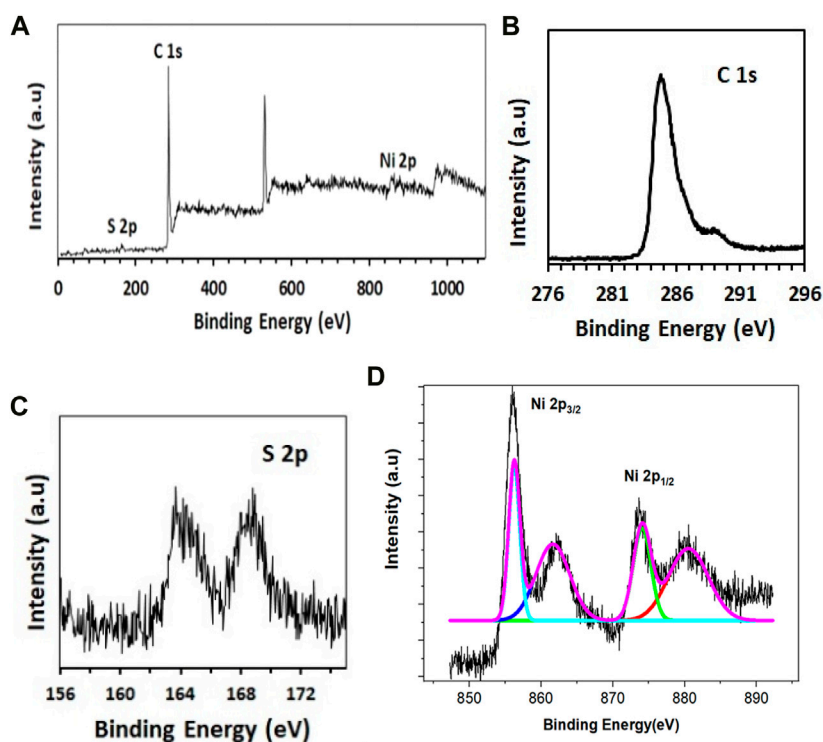


**FIGURE 2**  
XPS analysis of GO-Ni<sub>3</sub>S<sub>2</sub> nanocomposites. (A) Survey (B) C1s (C) S2s, and (D) Ni2p spectra.

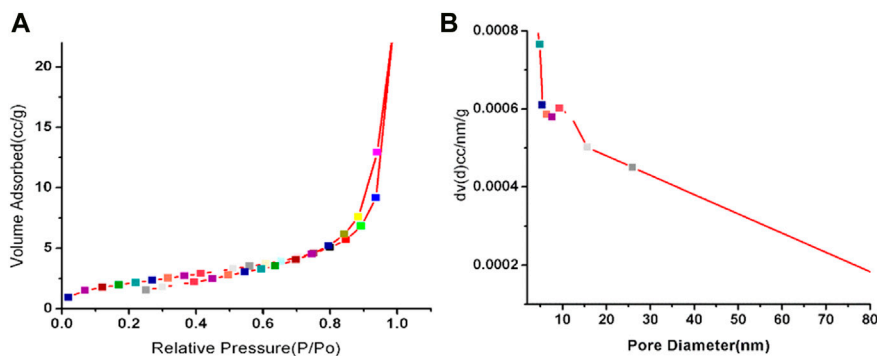


**FIGURE 3**  
Nitrogen adsorption/desorption isotherm at -196 °C (A) and the corresponding BJH pore size distribution plot (B) of GO-Ni<sub>3</sub>S<sub>2</sub> nanocomposites.

suggests electron transport resistance to the redox probe. The semicircle does not exist on the GO-Ni<sub>3</sub>S<sub>2</sub>@GCE, indicating a reduced barrier to electron transmission. This could be due to the high conductivity of GO-Ni<sub>3</sub>S<sub>2</sub> coated on the GCE (Zanello, 2003). The impedance charts are in accordance with that of CV behavior.

### 3.5 Simultaneous detection of dopamine and tyrosine on GO-Ni<sub>3</sub>S<sub>2</sub>@GCE

Figure 5 shows simultaneous detection tests of dopamine and tyrosine electrochemically. In the case of GO-Ni<sub>3</sub>S<sub>2</sub>@GCE with only

dopamine shows I<sub>pa</sub> (current) 0.0238275 mA at E<sub>pa</sub> (voltage) of 0.188155V (Figure 5D), and in the case of Ni<sub>3</sub>S<sub>2</sub>-GO/GCE with tyrosine shows I<sub>pa</sub> (current) 0.0211739 mA at E<sub>pa</sub> (voltage) 0.73622 V (Figure 5D). Furthermore, when the simultaneous detection of tyrosine and dopamine was carried out using 100 μM dopamine and 500 μM tyrosine in a PBS buffer solution at pH 7 (Figure 5F), two distinct oxidation peaks, with dopamine appearing at 0.245 V with a current 0.0116994 mA and tyrosine appearing at 0.7952 V with current 0.0161773 mA, respectively was observed. The experimental data clearly revealed that the GO-Ni<sub>3</sub>S<sub>2</sub>@GCE is capable of separating and differentiating the analytes dopamine and tyrosine.

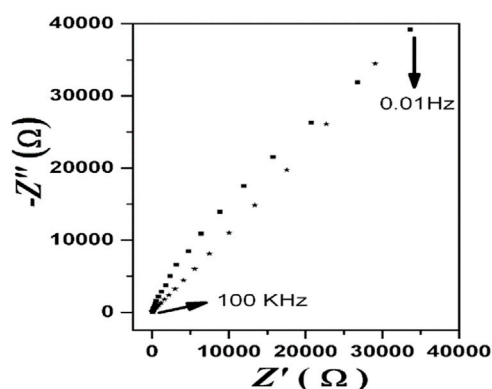


FIGURE 4

Nyquist impedance plots of (■) bare GCE and (∗) GO-Ni<sub>3</sub>S<sub>2</sub>@GCE in the frequency range 100 kHz to 100 mHz and the supporting electrolyte is 0.1 M KCl in 0.1 M PBS.

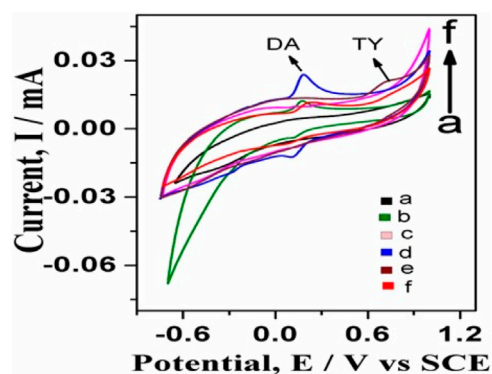


FIGURE 5

Simultaneous detection studies of dopamine and tyrosine on bare GCE and GO-Ni<sub>3</sub>S<sub>2</sub>@GCE: (A) bare GCE without any analyte, (B) bare GCE with dopamine, (C) GO-Ni<sub>3</sub>S<sub>2</sub>@GCE without analyte, (D) GO-Ni<sub>3</sub>S<sub>2</sub>@GCE with dopamine, (E) GO-Ni<sub>3</sub>S<sub>2</sub>@GCE with 500 μM tyrosine (F) GO-Ni<sub>3</sub>S<sub>2</sub>@GCE with dopamine 100 μM and tyrosine 500 μM at a scan rate of 50 mV/s.

The GO-Ni<sub>3</sub>S<sub>2</sub>@GCE shows a three-fold increase in the anodic peak current compared to bare GCE using dopamine as an analyte (Figure 5D) which in turn can be attributed to the improved electrochemical current responsiveness with increased conductivity and surface area after electrode surface modification. The electroactive area of bare GCE and GO-Ni<sub>3</sub>S<sub>2</sub>@GCE were calculated and compared using the Randles-Sevcik equation to establish that the surface area of GCE increases when modified with GO-Ni<sub>3</sub>S<sub>2</sub> (Laviron, 1979).

$$i_p = (2.69 \times 10^5) n^3 D^{1/2} v^{1/2} A c$$

The electrochemical areas calculated by using the equation are 0.112 cm<sup>2</sup> and 0.238 cm<sup>2</sup> for bare GCE and GO-Ni<sub>3</sub>S<sub>2</sub>@GCE respectively. There was a 50% increase in the electroactive surface area of modified GCE compared to that of bare GCE, in turn supporting the hypothesis.

### 3.6 Effect of scan rate on peak current of dopamine and tyrosine

The influence of scan rate on current and potential was studied, as indicated in Figure 6. The scan rate was varied from 50 to 400 mV s<sup>-1</sup> in a system consisting of dopamine in 0.1 M PBS at pH 7 using GO-Ni<sub>3</sub>S<sub>2</sub>@GCE. The peak current increased with a minor positive shift in peak potential in the 50–400 mV/s region. The regression equation expressed as  $I_{pa} = 0.00497 x + 0.01271$  ( $R^2 = 0.99719$ ) (for  $I_{pa}$  vs square root of scan rate) indicating that diffusion control process is governing the kinetic of the reaction and dopamine oxidation is a two-electron transfer process (Scheme 2).

Similarly, the cyclic voltammetry profiles were recorded to investigate the influence of scan rate on the electroactive surface of GO-Ni<sub>3</sub>S<sub>2</sub>@GCE taking tyrosine (500 μM) (Figure 6B). Using Randles—Sevcik equation, a plot of  $I_{pa}$  vs square root of scan rate (50–400 mV/s) shows excellent linearity with linear regression expression as  $I_{pa} = 0.00359 x - 0.00537$  with  $R^2 = 0.99812$  suggesting the diffusion-controlled process for the oxidation of tyrosine. The charge transfer coefficient for GO-Ni<sub>3</sub>S<sub>2</sub>@GCE was found to be 0.496, and the theoretical value is 0.5, indicating that the adsorption of reactants and intermediates onto the modified sensor is diffusion-controlled and irreversible with both dopamine and tyrosine analytes.

### 3.7 Effect of increasing concentration of dopamine and tyrosine at GO-Ni<sub>3</sub>S<sub>2</sub>@GCE

The cyclic voltammograms were recorded at different concentrations of dopamine (Figure 7A). The anodic peak current increased linearly with the increase in dopamine concentration. The modified GO-Ni<sub>3</sub>S<sub>2</sub>@GCE was found to be sensitive to both low and high concentrations of dopamine. At higher dopamine concentrations, another reduction peak was observed at -0.445 mV potential. Apart from dopamine's oxidation and reduction peaks, the third peak at -0.445 mV is due to the ring closure product (leucodopaminechrome) of dopamine-o-quinone (Jin et al., 2005). The effect of varying concentrations of tyrosine at modified GO-Ni<sub>3</sub>S<sub>2</sub>@GCE followed a similar trend as was seen with dopamine (Figure 7B). The oxidation peak at a tyrosine concentration of 500 μM was most prominent among the concentrations studied, and this concentration was therefore chosen for all further comparative studies.

### 3.8 Effect of pH on redox behavior of dopamine and tyrosine

The influence of pH on the oxidation of dopamine was studied at GO-Ni<sub>3</sub>S<sub>2</sub>@GCE in PBS buffer with varying pH ranging from 4 to 12 at a scan rate of 50 mV/s (Figure 8). It can be seen that the peak current and potential were strongly affected by pH, in turn indicating the involvement of protons in the electrode reactions. A good linear relationship between  $E_{pa}$  and pH was observed with the regression expression of  $E_{pa} = 0.049x + 0.49214$  with  $R^2 = 0.99258$ , the charge transfer coefficient “K” value of 0.049V/pH is close to the theoretical value of 0.059V/pH indicating that the

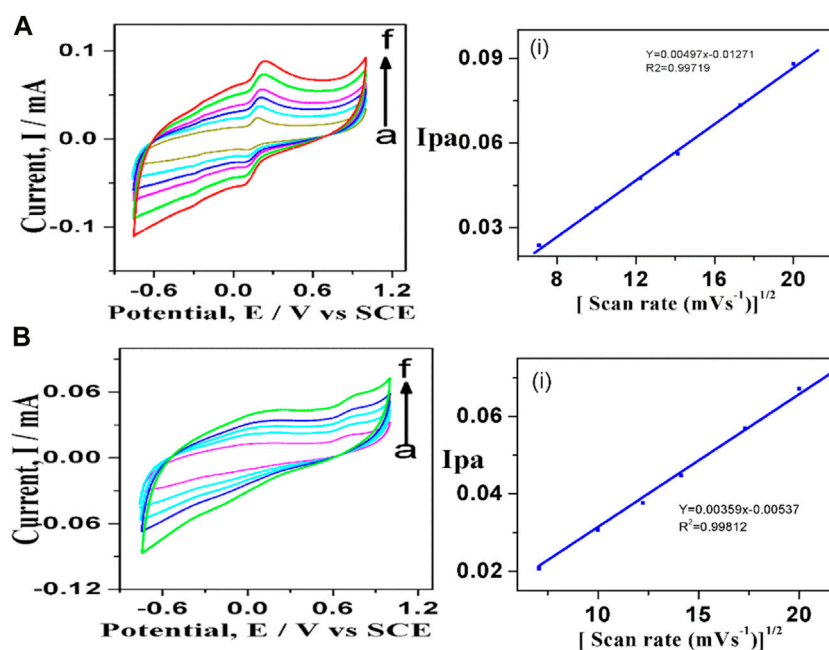
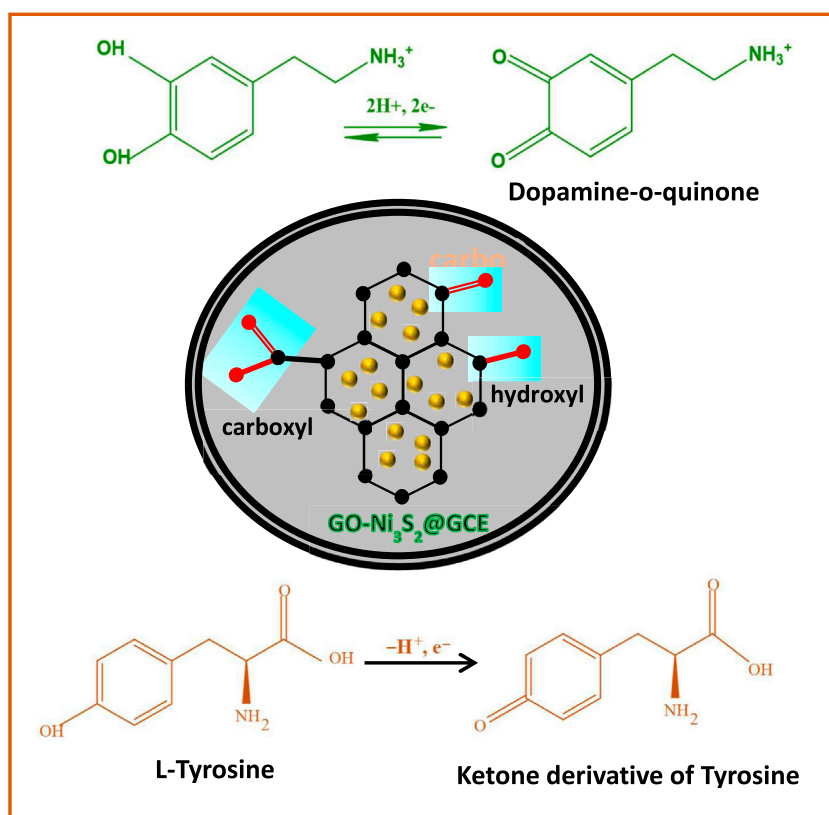


**FIGURE 6**  
Cyclic voltammograms recorded at different scan rates using (A) 100  $\mu\text{M}$  dopamine and (B) 500  $\mu\text{M}$  tyrosine at GO- $\text{Ni}_3\text{S}_2$ @GCE in 0.1 M PBS solution of pH 7: (A) 50, (B) 100, (C)150, (D) 200 e) 300, (F) 400 mV and (I)  $I_{pa}$  vs square root of scan rate.



**SCHEME 2**  
Plausible schematic representation of electrochemical reaction of L-tyrosine and dopamine on GO- $\text{Ni}_3\text{S}_2$ @GCE

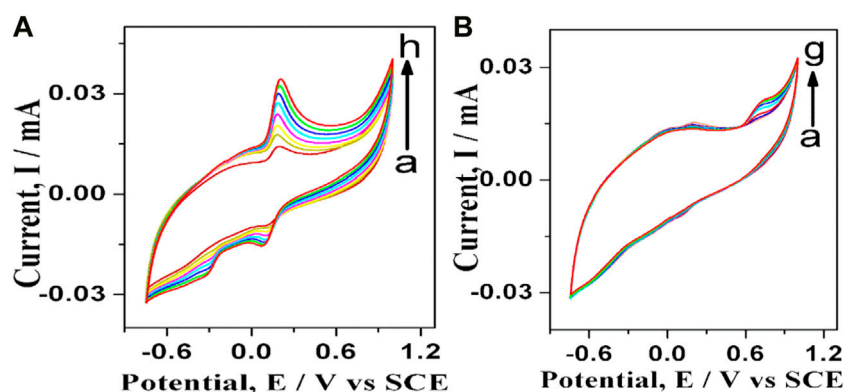


FIGURE 7

Cyclic voltammograms recorded at varying concentrations at GO-Ni<sub>3</sub>S<sub>2</sub>@GCE in PBS buffer of pH 7 (A) dopamine (A–H): (A) 25, (B) 50, (C) 75, (D) 100, (E) 125, (F) 150, (G) 200, (H) 250 μM and (B) Tyrosine: (A) 25, (B) 50, (C) 100, (D) 200, (E) 300, (F) 400, (G) 500 μM at 50 mV/s.

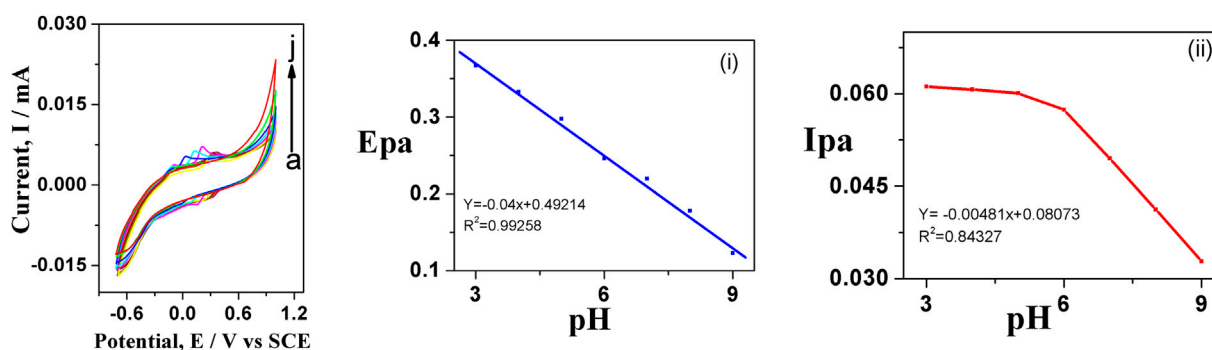


FIGURE 8

Cyclic voltammograms of (A) 100 μM dopamine with varying pH using 0.1 M PBS, scan rate 50 mV (A–J); (A) 4, (B) 5, (C) 6, (D) 7, (E) 8, (F) 9, (G) 10, (H) 11, (I) 12, (J) 13 at GO-Ni<sub>3</sub>S<sub>2</sub>@GCE

electron transfer process is accompanied by equal no of protons as given in Scheme 2.

The peak potential shifts to the negative side when pH is increased from 4 to 11, owing to enhanced reversibility of the oxidation, which involves deprotonation at elevated pH (Figure 8A). A similar trend was observed when using tyrosine as the analyte (figure not shown). Furthermore, the electrochemical response was found to be superior at pH = 7 PBS as desirable sensor applications in a wide range of areas.

The mechanism of detection of dopamine and tyrosine is shown in Scheme 2. In the PBS buffer solution at pH 7, the positively charged dopamine/tyrosine molecules can easily interact at the electrode surface through  $\pi$ - $\pi$  stacking or electrostatic attraction between the GO-Ni<sub>3</sub>S<sub>2</sub> and electrode to give the electrochemical response. The catalysts enhance the oxidation of dopamine to form dopaminophthalic acid and release two electrons and two protons. The faradic current generated by the flow of electrons at the surface of the electrode, in turn, depends upon the concentration of analyte. On the other hand, in the case of tyrosine, it is a single electron transfer as depicted in Scheme 2.

### 3.9 Chronoamperometric studies

The chronoamperometry investigations were carried out to understand the response nature of GO-Ni<sub>3</sub>S<sub>2</sub>@GCE to dopamine by adding 50 μM dopamine at intervals of 25 s in PBS solution containing 0.1M KCl (Figure 9). The response current was measured at a fixed potential of +0.25 V during stirring, and almost equivalent current steps were obtained for each addition of dopamine, indicating the catalytic efficacy of GO-Ni<sub>3</sub>S<sub>2</sub>@GCE. A linear relationship between peak current and dopamine concentration was obtained in the concentration range of  $2.5 \times 10^{-6}$  to  $270 \times 10^{-6}$  M, with the lowest detection limit being 12 nM. The determined limit of detection and sensitivity were compared with previously reported values, and the data is given in Table 1.

### 3.10 Interference studies

The interference studies on GO-Ni<sub>3</sub>S<sub>2</sub>@GCE were carried out by taking the common interfering biomolecules like uric acid and

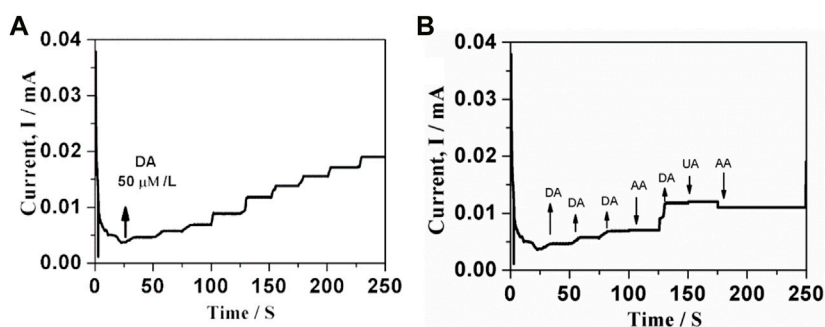


**FIGURE 9** Amperometry response of GO-Ni<sub>3</sub>S<sub>2</sub>@GCE for each addition of (A) 50 μM of dopamine (B) Interfering agents (i) 50 μM uric acid, (ii) 50 μM ascorbic acid at constant applied potential of +0.25 V in PBS containing 0.1 M KCl (pH 7.0).

**TABLE 1** Comparison of analytical performance at GO-Ni<sub>3</sub>S<sub>2</sub>@GCE with previously reported dopamine sensors.

S. No.	Modified electrode	LOD (μM)	Linear range (μM)	Ref
1	GN/GCE	1.5	3.3–249.1	Bu et al. (2013)
2	SGN/NiPc (Qi et al., 2016)	0.26	40–1,080	Barros et al. (2013)
3	N-G/NiTsPc/GCE	0.1	0.1–200	Xu et al. (2016)
4	PtCNC/MWCNT@GO/GCE	0.27	0.8–300	Zhang and Zheng (2020)
5	WS <sub>2</sub> NiS <sub>2</sub> -CNF/ITO	0.01	0.5–60	Yue et al. (2019)
6	Ni-CNT/GCE	0.044	0.05–100.05	Manivel et al. (2019)
7	CPE/Ni <sub>3</sub> -xTe <sub>2</sub>	0.15	4.0–31	Ulbrich et al. (2020)
8	GO-Ni <sub>3</sub> S <sub>2</sub> @GCE	0.012	2.5–270	Current work

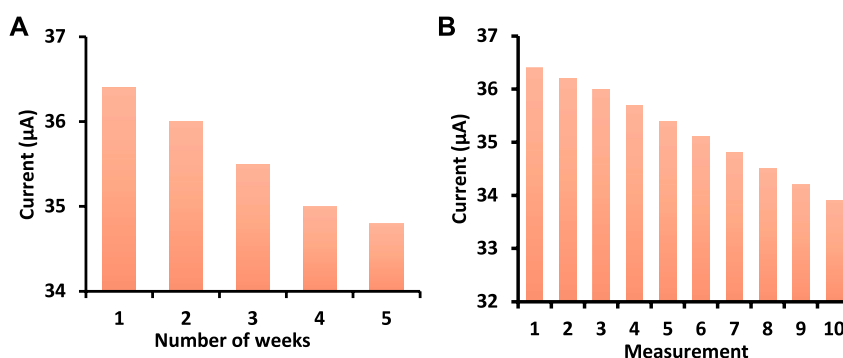


**FIGURE 10** (A) Stability and (B) Repeatability studies of GO-Ni<sub>3</sub>S<sub>2</sub>@GCE in PBS buffer at pH 7 containing 50 μM dopamine concentration at 50 mV/s scan rate.

ascorbic acid in phosphate buffer at pH 7.0 using the chronoamperometry (Figure 9B). The synthesized sensor system exhibited insignificant current intensity changes with respect to uric acid and ascorbic acid, highlighting the selectivity of GO-Ni<sub>3</sub>S<sub>2</sub>@GCE.

### 3.11 Stability and repeatability of GO-Ni<sub>3</sub>S<sub>2</sub>@GCE

The stability of GO-Ni<sub>3</sub>S<sub>2</sub>@GCE was assessed by immersing it in a PBS buffer solution with a pH of 7.0 for 3 weeks. The cyclic

voltgrams were recorded weekly and compared with that obtained on day one. After 3 weeks, the current drop was only 10%, illustrating the modified electrode's stability (Figure 10A).

The repeatability of the GO-Ni<sub>3</sub>S<sub>2</sub>@GCE was tested ten times with 100 μM dopamine. The modified electrode was washed with buffer solution after each measurement and analyzed for the same concentration (Figure 10B). The electrode's RSD (relative standard deviation) is 2.5%, indicating it is non-susceptible to surface fouling.

## 4 Conclusion

A facile and green synthesis of nickel-sulfide quantum dots using leaf extracts is demonstrated. The thus formed Ni<sub>3</sub>S<sub>2</sub> quantum dots are decorated on the exfoliated GO sheets *via* hydrothermal treatment to generate GO-Ni<sub>3</sub>S<sub>2</sub> nanocomposites. The GO-Ni<sub>3</sub>S<sub>2</sub> are then integrated on GCE by drop casting to form GO-Ni<sub>3</sub>S<sub>2</sub>@GCE. The modified electrode is further utilized to simultaneously detect dopamine and tyrosine electrochemically. The effect of dopamine and tyrosine concentration, scan rate and pH on peak current is well studied to deduce a plausible mechanism of oxidation of dopamine and tyrosine. It is found that dopamine oxidation is a two-electron transfer, whereas tyrosine oxidation is accompanied by a one-electron transfer. The GO-Ni<sub>3</sub>S<sub>2</sub>@GCE is stable for 3 weeks with a current drop of only 10%. The lowest detection limit of dopamine is obtained by taking ten blank experiments without analyte and from a calibration plot we get the standard deviation (SD) and slope. LOD is calculated using the formula  $LOD = 3 \times SD/slope$  and found to be 12 nM indicating the efficacy of GO-Ni<sub>3</sub>S<sub>2</sub>@GCE. This work solves the effect of AA on the EC detection of DA, which is promising in practical applications, such as precisely monitoring DA levels in biological systems and quantifying DA in complex samples. Future research may use *in situ* spectral characterization to

gain deeper understanding of the real function of nickel sulphides in the electrochemical analysis. Another issue is how to efficiently increase the nickel sulphide charge transfer rate in electrochemical sensing.

## Data availability statement

The raw data supporting the conclusion of this article will be made available by the authors, without undue reservation.

## Author contributions

MH carried out the experiments, AR conceived, planned and analysed the results, MN and GB contributed in interpretation and writing the manuscript the GR helped in characterization of the samples. All authors contributed to the article and approved the submitted version.

## Conflict of interest

The authors declare that the research was conducted in the absence of any commercial or financial relationships that could be construed as a potential conflict of interest.

## Publisher's note

All claims expressed in this article are solely those of the authors and do not necessarily represent those of their affiliated organizations, or those of the publisher, the editors and the reviewers. Any product that may be evaluated in this article, or claim that may be made by its manufacturer, is not guaranteed or endorsed by the publisher.

## References

- Alonso, S., Zamora, L., and Calatayud, M. (2003). Determination of tyrosine through a FLA-direct chemiluminescence procedure. *Talanta* 60, 369–376. doi:10.1016/S0039-1404(03)00099-7
- Barros, S. B. A., Rahim, A., Tanaka, A. A., Arenas, L. T., Landers, R., and Gushikem, Y. (2013). *In situ* immobilization of nickel(II) phthalocyanine on mesoporous SiO<sub>2</sub>/C carbon ceramic matrices prepared by the sol-gel method: Use in the simultaneous voltammetric determination of ascorbic acid and dopamine. *Electrochim. Acta* 87, 140–147. doi:10.1016/j.electacta.2012.09.012
- Bhakta, A. K., Mascarenhas, R. J., D'Souza, O. J., Satpati, A. K., Detriche, S., Mekhalif, Z., et al. (2015). Iron nanoparticles decorated multi-wall carbon nanotubes modified carbon paste electrode as an electrochemical sensor for the simultaneous determination of uric acid in the presence of ascorbic acid, dopamine and L-tyrosine. *Mater. Sci. Eng. C* 57, 328–337. doi:10.1016/j.msec.2015.08.003
- Bu, Y., Dai, W., Li, N., Zhao, X., and Zuo, X. (2013). The graphene nanopowder for electro-catalytic oxidation of dopamine and uric acid in the presence of ascorbic acid. *J. Energy Chem.* 22, 685–689. doi:10.1016/s2095-4956(13)60091-1
- Carrera, V., Sabater, E., Vilanova, E., and Sogorb, M. A. (2007). A simple and rapid HPLC-MS method for the simultaneous determination of epinephrine, norepinephrine, dopamine and 5-hydroxytryptamine: Application to the secretion of bovine chromaffin cell cultures. *J. Chromatogr. B* 847, 88–94. doi:10.1016/j.jchromb.2006.09.032
- Chen, J. L., Yan, X. P., Meng, K., and Wang, S. F. (2011). Graphene oxide based photoinduced charge transfer label-free near-infrared fluorescent biosensor for dopamine. *Anal. Chem.* 83, 8787–8793. doi:10.1021/ac2023537
- Cheng, J., Wang, X., Nie, T., Yin, L., Wang, S., Zhao, Y., et al. (2020). A novel electrochemical sensing platform for detection of dopamine based on gold nanobipyramid/multi-walled carbon nanotube hybrids. *Anal. Bioanal. Chem.* 412, 2433–2441. doi:10.1007/s00216-020-02455-5
- Cheng, M., Zhang, X., Wang, M., Huang, H., and Ma, J. (2017). A facile electrochemical sensor based on well-dispersed graphenemolybdenum disulfide modified electrode for highly sensitive detection of dopamine. *J. Electroanal. Chem.* 786, 1–7. doi:10.1016/j.jelechem.2017.01.012
- Cheng, N., Liu, Q., Asiri, A. M., Xing, W., and Sun, X. (2015). A Fe-doped Ni<sub>3</sub>S<sub>2</sub> particle film as a high-efficiency robust oxygen evolution electrode with very high current density. *J. Mat. Chem. A* 3, 23207–23212. doi:10.1039/c5ta06788j
- Dalley, J. W., and Roiser, J. P. (2012). Dopamine, serotonin and impulsivity. *Neuroscience* 215, 42–58. doi:10.1016/j.neuroscience.2012.03.065
- Danielle, W. K., Gabriel, L. B., Mika, E. M., and David, E. C. (2012). Electrochemical sensors and biosensors. *Anal. Chem.* 84, 685–707. doi:10.1021/ac202878q
- Devi, N. R., Kumar, T. V., and Sundramoorthy, A. K. (2018). Electrochemically exfoliated carbon quantum dots modified electrodes for detection of dopamine neurotransmitter. *J. Electrochem. Soc.* 165, G3112–G3119. doi:10.1149/2.0191812jes
- Dong, S., Zhang, P., Liu, H., Li, N., and Huang, T. (2011). Direct electrochemistry and electrocatalysis of hemoglobin in composite film based on ionic liquid and NiO microspheres with different morphologies. *Biosens. Bioelectron.* 26, 4082–4087. doi:10.1016/j.bios.2011.03.039
- Fazio, E., Spadaro, S., Bonsignore, M., Lavanya, N., Sekar, C., Leonardi, S., et al. (2018). Molybdenum oxide nanoparticles for the sensitive and selective detection of dopamine. *J. Electroanal. Chem.* 814, 91–96. doi:10.1016/j.jelechem.2018.02.051

- Ferguson, A. A., Roy, S., Kaitlyn, N. K., Yongsoo, K., Dumas, K. J., Ritov, V. B., et al. (2013). TATN-1 mutations reveal a novel role for tyrosine as a metabolic signal that influences developmental decisions and longevity in *Caenorhabditis elegans*. *PLoS Genet.* 9 (12), 1–22. doi:10.1371/journal.pgen.1004020
- Furukawa, Y., and Kish, S. (2008). “Tyrosine hydroxylase deficiency,” in *GeneReviews*® [internet]. Editors M. P. Adam, H. H. Ardinger, and R. A. Pagon. 1st ed (Seattle, USA: University of Washington), 1–21.
- Gao, F., Liu, L., Cui, G., Xu, L., Wu, X., Kuang, H., et al. (2017). Regioselective plasmonic nano-assemblies for bimodal subfemtomolar dopamine detection. *Nanoscale* 9, 223–229. doi:10.1039/C6NR08264E
- Gao, Z., Chen, C., Chang, J., Chen, L., Wang, P., Wu, D., et al. (2018). Porous Co<sub>3</sub>S<sub>4</sub>@Ni<sub>3</sub>S<sub>4</sub> heterostructure arrays electrode with vertical electrons and ions channels for efficient hybrid supercapacitor. *Chem. Eng. J.* 343, 572–582. doi:10.1016/j.cej.2018.03.042
- Ghods, J., Rafati, A. A., Shoja, Y., and Najafi, M. (2015). Determination of dopamine in the presence of uric acid and folic acid by carbon paste electrode modified with CuO nanoparticles/hemoglobin and multi-walled carbon nanotube. *J. Electrochem. Soc.* 162, B69–B74. doi:10.1149/2.0491504jes
- Govindasamy, M., Alothman, Z. A., Alshgari, R. A., Arumugam, R., and Huang, C.-H. (2023). Highly efficient electrocatalytic oxidation of hexestrol based on bismuth molybdenum oxide nanoparticle/graphene oxide nanosheets modified screen printed electrode. *J. Environ. Chem. Eng.* 11 (3), 109680. doi:10.1016/j.jece.2023.109680
- Govindasamy, M., Wang, S.-F., Bowya, S., Ramalingam, R. J., Al-lohedan, H., and Sathiyane, A. (2019). A novel electrochemical sensor for determination of DNA damage biomarker (8-hydroxy-2'-deoxyguanosine) in urine using sonochemically derived graphene oxide sheets covered zinc oxide flower modified electrode. *Ultrason. Sonochemistry* 58, 104622. doi:10.1016/j.ulsonch.2019.104622
- Hou, L., Shi, Y., Zhu, S., Rehan, M., Pang, G., Zhang, X., et al. (2017). Hollow mesoporous hetero-NiCo<sub>2</sub>S<sub>4</sub>/Co<sub>9</sub>S<sub>8</sub> submicro-spindles: Unusual formation and excellent pseudo-capacitance towards hybrid supercapacitors. *J. Mat. Chem. A* 5, 133–144. doi:10.1039/c6ta05788h
- How, G. T. S., Pandikumar, A., Ming, H. N., and Ngee, L. H. (2014). Highly exposed {001} facets of titanium dioxide modified with reduced graphene oxide for dopamine sensing. *Sci. Rep.* 4, 5044–5048. doi:10.1038/srep05044
- Huang, F., Peng, Y., Jin, G., Zhang, S., and Kong, J. (2008). Sensitive detection of haloperidol and hydroxyzine at multi-walled carbon nanotubes-modified glassy carbon electrodes. *Sensors* 8, 1879–1889. doi:10.3390/s8031879
- Huang, Y., Jiang, X. Y., Wang, W., Duan, J. P., and Chen, G. (2006). Separation and determination of L-tyrosine and its metabolites by capillary zone electrophoresis with a wall-jet amperometric detection. *Talanta* 70, 1157–1163. doi:10.1016/j.talanta.2006.03.009
- Ishii, Y., Iijima, M., Umemura, T., Nishikawa, A., Iwasaki, Y., Ito, R., et al. (2006). Determination of nitrotyrosine and tyrosine by high-performance liquid chromatography with tandem mass spectrometry and immunohistochemical analysis in livers of mice administered acetaminophen. *J. Pharm. Biomed. Anal.* 41, 1325–1331. doi:10.1016/j.jpba.2006.02.045
- Jackowska, K., and Kryszynski, P. (2013). New trends in the electrochemical sensing of dopamine. *Anal. Bioanal. Chem.* 405, 3753–3771. doi:10.1007/s00216-012-6578-2
- Jayaprakash, G. K., Swamy, B. E. K., Sánchez, J. P. M., Li, X., Sharma, S. C., and Lee, S. L. (2020). Electrochemical and quantum chemical studies of cetylpyridinium bromide modified carbon electrode interface for sensor applications. *J. Mol. Liq.* 315, 113719. doi:10.1016/j.molliq.2020.113719
- Jin, G., Zhang, Y., and Cheng, W. (2005). Poly (p-aminobenzene sulfonic acid)-modified glassy carbon electrode for simultaneous detection of dopamine and ascorbic acid. *Sens. Actuators B* 107, 528–534. doi:10.1016/j.snb.2004.11.018
- Kapalka, G. (2010). “Chapter 4: Substances involved in neurotransmission,” in *Nutritional and herbal therapies for children and adolescents*. 1st Ed. (London, UK: Academic Press is an imprint of Elsevier), 74–99. doi:10.1016/C2009-0-01890-X
- Khadjavi, A., Mannu, F., Destefanis, P., Sacerdote, C., Battaglia, A., Allasia, M., et al. (2015). Early diagnosis of bladder cancer through the detection of urinary tyrosine-phosphorylated proteins. *Br. J. Cancer* 113, 469–475. doi:10.1038/bjc.2015.232
- Khan, S., Mahmood, A., Ali Shah, A. U. H., Rahman, G., and Khan, A. (2022). Nabi Ullah Challenges and innovative strategies related to synthesis and electrocatalytic/energy storage applications of metal sulfides and its derivatives. *J. Electroanal. Chem.* 923, 1–16760. doi:10.1016/j.jelechem.2022.116760
- Khattar, R., and Mathur, P. (2013). 1-(Pyridin-2-ylmethyl)-2-(3-(1-(pyridin-2-ylmethyl)benzimidazol-2-yl) propyl) benzimidazole and its copper(II) complex as a new fluorescent sensor for dopamine (4-(2-aminoethyl)benzene-1,2-diol). *Inorg. Chem. Commun.* 31, 37–43. doi:10.1016/j.inoche.2013.02.015
- Kim, D. S., Kang, E. S., Baek, S., Choo, S. S., Chung, Y. H., Lee, D., et al. (2018). Electrochemical detection of dopamine using periodic cylindrical gold nanoelectrode arrays. *Sci. Rep.* 8, 14049–14110. doi:10.1038/s41598-018-32477-0
- Laviron, E. (1979). General expression of the linear potential sweep voltammogram in the case of diffusion less electrochemical systems. *J. Electroanal. Chem. Interfacial Electrochem.* 101, 19–28. doi:10.1016/S0022-0728(79)80075-3
- Lee, C. J., and Yang, J. (2006).  $\alpha$ -Cyclodextrin-modified infrared chemical sensor for selective determination of tyrosine in biological fluids. *Anal. Biochem.* 359, 124–131. doi:10.1016/j.ab.2006.09.004
- Leng, Y., Xie, K., Ye, L., Li, G., Lu, Z., and He, J. (2015). Goldnanoparticle-based colorimetric array for detection of dopamine in urine and serum. *Talanta* 139, 89–95. doi:10.1016/j.talanta.2015.02.038
- Liu, B., Luo, L., Ding, Y., Si, X., Wei, Y., Ouyang, X., et al. (2014). Differential pulse voltammetric determination of ascorbic acid in the presence of folic acid at electro-deposited NiO/graphene composite film modified electrode. *Electrochim. Acta* 142, 336–342. doi:10.1016/j.electacta.2014.07.126
- Manivel, P., Thamilselvan, A., Rajagopal, V., Nesakumar, N., and Suryanarayanan, V. (2019). Enhanced electrocatalytic activity of Ni-CNT nanocomposites for simultaneous determination of epinephrine and dopamine. *Electroanalysis* 31, 2387–2396. doi:10.1002/elan.201900201
- Manjunatha, H., Nagaraju, D. H., Suresh, G. S., and Venkatesha, T. V. (2009). Detection of uric acid in the presence of dopamine and high concentration of ascorbic acid using PDDA modified graphite electrode. *Electroanalysis* 21, 2198–2206. doi:10.1002/elan.200904662
- Mohorko, N., Petelin, A., Jurdana, M., Gianni, B., and PraDnikar, Z. J. (2015). Elevated serum levels of cysteine and tyrosine: Early biomarkers in asymptomatic adults at increased risk of developing metabolic syndrome. *BioMed Res. Int.* 2015, 1–14. doi:10.1155/2015/418681
- Nurzulika, R., Lim, H. N., Harrison, I., Lim, S. S., Pandikumar, A., Huang, N. M., et al. (2015). Graphene/SnO<sub>2</sub> nanocomposite-modified electrode for electrochemical detection of dopamine. *Sens. Biosens. Res.* 5, 42–49. doi:10.1016/j.sbsr.2015.06.002
- Owesson-White, C. A., Roitman, M. F., Sombers, L. A., Belle, A. M., Keithley, R. B., Peele, J. L., et al. (2012). Sources contributing to the average extracellular concentration of dopamine in the nucleus accumbens. *J. Neurochem.* 121, 252–262. doi:10.1111/j.1471-4159.2012.07677.x
- Qi, D., Zhang, Q., Zhou, W., Zhao, J., Zhang, B., Sha, Y., et al. (2016). Quantification of dopamine in brain microdialysates with high-performance liquid chromatography–tandem mass spectrometry. *Anal. Sci.* 32, 419–424. doi:10.2116/analsci.32.419
- Rajaji, U., Raghu, M. S., Yogesh Kumar, K., Al-Kahtani, A. A., Chen, C. P., Juang, R. S., et al. (2022). Electrocatalytic oxidation and amperometric determination of sulfasalazine using bimetal oxide nanoparticles–decorated graphene oxide composite modified glassy carbon electrode at neutral pH. *Mikrochim. Acta* 189 (11), 409. doi:10.1007/s00604-022-05498-w
- Rajaji, U., Nair, J. S. A., Chen, S.-M., Sandhya, K. Y., Alshgari, R. A., and Jiangad, T.-Y. (2021). A disposable electrode modified with metal orthovanadate and sulfur-reduced graphene oxide for electrochemical detection of anti-rheumatic drug. *New J. Chem.* 45, 19858–19867. doi:10.1039/D1NJ02775A
- Schumacher, F., Chakraborty, S., Kleuser, B., Gulbins, E., Schwerdtle, T., Aschner, M., et al. (2015). Highly sensitive isotope-dilution liquid chromatography–electrospray ionization–tandem-mass spectrometry approach to study the drug-mediated modulation of dopamine and serotonin levels in *Caenorhabditis elegans*. *Talanta* 144, 71–79. doi:10.1016/j.talanta.2015.05.057
- Shen, J., Sun, C., and Wu, X. (2017). Silver nanoprisms-based Tb (III) fluorescence sensor for highly selective detection of dopamine. *Talanta* 165, 369–376. doi:10.1016/j.talanta.2016.12.073
- Tamilalagan, E., Akilarasan, M., Chen, S., Govindasamy, M., Lin, K.-Y., Mohammed Alzahrani, F., et al. (2023). Construction of perovskite structured ZnSnO<sub>3</sub> embedded graphene oxide nanosheets for *in-situ* electrochemical quantification of organoarsenic roxarsone. *Process Saf. Environ. Prot.* 171, 705–716. doi:10.1016/j.psep.2023.01.042
- Tian, Z., Yin, J., Wang, X., and Wang, Y. (2019). Construction of Ni<sub>3</sub>S<sub>2</sub> wrapped by rGO on carbon cloth for flexible supercapacitor application. *J. Alloys Compd.* 777, 806–811. doi:10.1016/j.jallcom.2018.10.119
- Tooley, C. A., Gasperoni, C. H., and MarnotoHalpern, S. J. M. (2018). Evaluation of metal oxide surface catalysts for the electrochemical activation of amino acids. *Sensors* 18, 1–10. doi:10.3390/s18093144
- Tseng, T.-W., Rajaji, U., Chen, T.-W., Chen, S.-M., Huang, Y. C., Veerappan Mania, A., et al. (2020). Sonochemical synthesis and fabrication of perovskite type calcium titanate interfacial nanostructure supported on graphene oxide sheets as a highly efficient electrocatalyst for electrochemical detection of chemotherapeutic drug. *Ultrason. Sonochemistry* 69, 105242. doi:10.1016/j.ulsonch.2020.105242
- Turyan, I., Frenkel, R., and Sosic, Z. (2018). Rapid quantification of tyrosine sulfation in therapeutic proteins. *Anal. Biochem.* 549, 96–98. doi:10.1016/j.ab.2018.03.001
- Üge, A., Zeybek, D. K., and Zeybek, B. (2018). An electrochemical sensor for sensitive detection of dopamine based on MWCNTs/CeO<sub>2</sub>PEDOT composite. *J. Electroanal. Chem.* 813, 134–142. doi:10.1016/j.jelechem.2018.02.028
- Ulbrich, K. F., Winiarski, J. P., Jost, C. L., and de Campos, C. E. M. (2020). Mechanochemical synthesis of a Ni<sub>3</sub>-xTe<sub>2</sub> nanocrystalline composite and its application for simultaneous electrochemical detection of dopamine and adrenaline. *Compos. Part B Eng.* 183, 107649. doi:10.1016/j.compositesb.2019.107649
- Wan, Q. L., and Zhiqiang, G. (2015). Metal oxide nanoparticles in electroanalysis. *Electroanalysis* 27, 1–18. doi:10.1002/elan.201500024

- Wu, P., Wang, D., Ning, J., Zhang, J., Feng, X., Dong, J., et al. (2018). Novel 3D porous graphene/Ni<sub>3</sub>S<sub>2</sub> nanostructures for high-performance supercapacitor electrodes. *J. Alloys Compd.* 731, 1063–1068. doi:10.1016/j.jallcom.2017.10.060
- Xia, X., Shen, X., Du, Y., Ye, W., and Wang, C. (2016). Study on glutathione's inhibition to dopamine polymerization and its application in dopamine determination in alkaline environment based on silver selenide/molybdenum selenide/glassy carbon electrode. *Sens. Actuators B* 237, 685–692. doi:10.1016/j.snb.2016.06.154
- Xu, H., Xiao, J., Yan, L., Zhu, L., and Liu, B. (2016). An electrochemical sensor for selective detection of dopamine based on nickel tetrasulfonated phthalocyanine functionalized nitrogen-doped graphene nanocomposites. *J. Electroanal. Chem.* 779, 92–98. doi:10.1016/j.jelechem.2016.04.032
- Yang, J., Yu, J. H., Strickler, J. R., Chang, W. J., and Gunasekaran, S. (2013). Nickel nanoparticle-chitosan-reduced graphene oxidemodified screen-printed electrodes for enzyme-free glucose sensing in portable microfluidic devices. *Biosens. Bioelectron.* 47, 530–538. doi:10.1016/j.bios.2013.03.051
- Yang, L., Wang, G., Liu, Y., and Wang, M. (2013). Development of a biosensor based on immobilization of acetylcholinesterase on NiO nanoparticles-carboxylic graphene-nafion modified electrode for detection of pesticides. *Talanta* 113, 135–141. doi:10.1016/j.talanta.2013.03.025
- Yang, X., Zhao, L., and Lian, J. (2017). Arrays of hierarchical nickel sulfides/MoS<sub>2</sub> nanosheets supported on carbon nanotubes backbone as advanced anode materials for asymmetric supercapacitor. *J. Power Sour.* 343, 373–382. doi:10.1016/j.jpowsour.2017.01.078
- Yue, H. Y., Wu, P. F., Huang, S., Gao, X., Song, S. S., Wang, W. Q., et al. (2019). Electrochemical determination of dopamine in the presence of uric acid using WS<sub>2</sub> nanospherescarbon nanofibers. *J. Electroanal. Chem.* 833, 427–432. doi:10.1016/j.jelechem.2018.12.016
- Zahra, T. A., Oana, H., Cecilia, C., Mohammad, M. A., and Giovanna, M. (2019). Latest trends in electrochemical sensors for neurotransmitters: A review. *Sensors* 19, 1–30. doi:10.3390/s19092037
- Zanello, P. (2003). *Inorganic electrochemistry: Theory, practice and application*. London, United Kingdom: The Royal Society of Chemistry. ISBN 0-85404-661-5.
- Zhang, X., and Zheng, J. (2020). High-index {hk0} facets platinum concave nanocubes loaded on multiwall carbon nanotubes and graphene oxide nanocomposite for highly sensitive simultaneous detection of dopamine and uric acid. *Talanta* 207, 120296. doi:10.1016/j.talanta.2019.120296
- Zhao, J., Guan, B., Hu, B., Xu, Z., Wang, D., and Zhang, H. (2017). Vulcanizing time controlled synthesis of NiS microflowers and its application in asymmetric supercapacitors. *Electrochimica Acta* 230, 428–437. doi:10.1016/j.electacta.2017.02.032
- Zhao, J., Zhang, Y., Wang, Y., Li, H., and Peng, Y. (2018). The application of nanostructured transition metal sulfides as anodes for lithium ion batteries. *J. Energy Chem.* 27 (6), 1536–1554. doi:10.1016/j.jechem.2018.01.009
- Zhou, S., Huang, Y., Xu, L., and Wen, Z. (2018). Microwave-assisted synthesis of graphene-NiS/Ni<sub>3</sub>S<sub>2</sub> composites for enhanced microwave absorption behaviors through a sulfuration method. *Ceramics International* 44, 21786–21793. doi:10.1016/j.ceramint.2018.08.281
- Zou, X., Sun, Q., Zhang, Y., Li, G. -D., Liu, Y., Wu, Y., et al. (2018). Ultrafast surface modification of Ni<sub>3</sub>S<sub>2</sub> nanosheet arrays with Ni-Mn bimetallic hydroxides for high-performance supercapacitors. *Sci. Rep.* 8, 4478. doi:10.1038/s41598-018-22448-w